Annals of Biomedical Engineering, Vol. 16, pp. 547-571, 1988
Printed in the USA.

0090-6964/88 $3.00 + .00

DYNAMICS OF HEAT, WATER, AND SOLUBLE GAS EXCHANGE IN THE HUMAN AIRWAYS: 1. A MODEL STUDY

Maria E. Tsu, Albert L. Babb, David D. Ralph, and Michael P. Hlastala

University of Washington
Departments of Chemical Engineering, Medicine, and of Physiology and Biophysics

(Received 6/18/87; Revised 4/29/88)

In order to provide a means for analysis of heat, water, and soluble gas exchange with the airways during tidal ventilation, a one dimensional theoretical model describing heat and water exchange in the respiratory airways has been extended to include soluble gas exchange with the airway mucosa and water exchange with the mucous layer lining the airways. Not only do heat, water, and gas exchange occur simultaneously, but they also interact. Heating and cooling of the airway surface and mucous lining affects both evaporative water and soluble gas exchange. Water evaporation provides a major source of heat exchange. The model-predicted mean airway temperature profiles agree well with literature data for both oral and nasal breathing validating that part of the model. With model parameters giving the best fit to experimental data, the model shows: (a) substantial heat recovery in the upper airways, (b) minimal respiratory heat and water loss, and (c) low average mucous temperatures and maximal increases in mucous thickness. For resting breathing of room air, heat and water conservation appear to be more important than conditioning efficiency. End-tidal expired partial pressures of very soluble gases eliminated by the lungs are predicted to be lower than the alveolar partial pressures due to the absorption of the expired gases by the airway mucosa. The model may be usable for design of experiments to examine mechanisms associated with the local hydration and dehydration dynamics of the mucosal surface, control of bronchial perfusion, triggering of asthma, mucociliary clearance and deposition of inhaled pollutant gases.

Keywords—*Airway exchange model, Soluble gas exchange, Respiratory air conditioning, Respiratory heat and water conservation, Respiratory mucous hydration dynamics.*

INTRODUCTION

The respiratory airways play several important roles in mammalian respiration: (a) the airways heat and humidify the inspired air, protecting the delicate alveolar tissue from dehydration (3,11), (b) the surfaces of the airway mucosa, cooled by the

This work was supported in part by Grant No. HL24163 of the National Institutes of Health.
Address correspondence to Dr. Albert L. Babb, Dept. of Chem. Eng., BF-10, University of Washington, Seattle, WA 98195.

sensible heat lost by conduction and convection and the latent heat lost by evaporation, recover heat and water from the expired air, conserving body heat and regulating temperature (17,22), and (c) the sticky mucous gel coating the airway surfaces traps inhaled microorganisms and pollutant particles and clears them from the airways, acting as an immuno-defense mechanism.

In addition to conditioning and filtering the inspired air, the airways participate in gas exchange between the airway lumen and the bronchial circulation. Although bronchial gas exchange contributes minimally to overall pulmonary gas exchange for the healthy lung in the absence of any environmental or physiological challenges, changes in bronchial circulation in response to common physiological stimuli or in compensation for decreased pulmonary blood flow in disease, coupled with the heat and water exchange between respired air and airway mucosa influence the exchange of gases. The significance of this gas exchange will depend on three factors: (a) the solubility of the gas, (b) the temperature dependence of the gas solubility, and (c) the degree of cooling experienced by the airway mucosa which in turn is affected by the breathing pattern and inspired air conditions.

This study focuses on the exchange of heat, water, and a soluble gas between the respired gas and airway mucosa. The bronchial exchange of soluble gases is relevant to understanding the consequence of inhaling pollutant gases, the effectiveness of aerosol therapy, and the exchange properties of soluble inert gases used in methods to characterize lung function such as the multiple inert gas elimination technique, MIGET (29). Recent studies of gas exchange during high frequency ventilation (16,20) suggest that the capacitance of the tissues of the conducting airways can significantly enhance the elimination of soluble infused inert gases. Thus, the study of the interaction of a soluble gas with the airway mucosa may allow a more accurate interpretation of inert gas exchange data.

While *in vivo* experimentation remains the primary means of obtaining information, mathematical modeling is a valuable tool which aids in the interpretation and contributes to the overall understanding of the dynamic events observed in the living system. Recent efforts to mathematically model transport phenomena occurring in the conducting airways (7,12,13,15,21) were limited to heat and water exchange with the mucosal surface with less attention given to events occurring in the airway mucosa. In this study, a one-dimensional mathematical model was developed to describe the dynamic heat and gas exchange processes occurring in the airways. The current model incorporates three new features: (a) the exchange of a soluble gas between the respired air and the airway mucosa, (b) a mucous layer which expands or contracts when either condensation or evaporation, respectively, takes place, and (c) the secretion of fluid from the tissue to the mucus as liquid evaporates from the airway surface.

This paper describes the mathematical model in some detail, deriving the major equations and briefly describing the numerical solution methods. By comparing the model predictions to available literature data, the model parameters giving the best fit are selected. The model is used to investigate airway conditioning efficiency, water and heat conservation, mucous layer dynamics, and soluble gas exchange during quiet tidal breathing and hyperpnea of room air. The sensitivity of the model predictions to changes in the model parameters is examined. Subsequent papers will investigate more fully the effects of breathing pattern and inspired air conditions on the dynamic airway exchange of heat, water, and soluble gases.

MODEL DEVELOPMENT

Air enters the respiratory airways through the nose or mouth, passes into the pharynx and through the larynx before entering the trachea (26). The trachea branches into the two main bronchi, which lead to the right and left lungs. Each bronchus bifurcates up to twenty-two more times into smaller and smaller airways, terminating in the alveolar region of the lung. The airway wall tissue contains a rich supply of blood vessels, lymph vessels, and nerves (18). Numerous mucous glands are imbedded in the tissue. Ciliated epithelial cells line the airway surface and continually move the mucus, secreted by the mucous glands, toward the pharynx. The mucus consists of long glycoprotein molecules, which form the framework of the gel, and other inorganic ionic species. Recent studies of the mucous gel propose that the mucous glands secrete concentrated packages of mucins which undergo spontaneous swelling, and that gel hydration is controlled by membrane transport of ions and water in a Donnan type equilibrium process (23,28).

Mathematical modeling of any system, especially biological ones, necessarily requires abstraction and simplification. The goal is not so much to reproduce the real system in detail but to include the major aspects of the real system that influence the processes of interest. Two alternative approaches have been used to model the heat, water, and soluble gas transport processes occurring in the human airways: (a) that taken by Kruse (15,21) which uses detailed continuity and energy balance equations, and (b) that taken by Hanna (7) and Ingenito (12,13) which uses a control volume analysis. The control volume analysis offers several advantages over the detailed analysis: (a) detailed knowledge of the velocity flow field is not required, (b) complicated geometries are more easily handled, (c) semi-empirical expressions for the rates of heat and mass transport are used which allow "fine tuning" of the model, and (d) greater detail can always be incorporated into successive versions of the model. For those reasons, the control volume analysis approach was taken.

Control Volume Description of Airway

Figure 1 depicts a cylindrical control volume in an airway with radius R positioned axially a distance z from the airway entrance. The airway is radially divided into three regions: the airway lumen, a thin mucous layer of thickness ΔR_1 coating the airway wall, and an underlying nonperfused tissue layer of thickness ΔR_2. A capillary bed lies beyond the nonperfused tissue layer and has an assumed temperature profile $T_c(z)$ and blood alcohol mole fraction profile $x_{Ac}(z)$. The variables describing temperature and concentration in each region are bulk average values for the entire region. The gas in the airway is treated as a ternary system of dry air, water vapor, and one soluble gas and is assumed to behave ideally. The model only considers the exchange of water and soluble gas with the airway mucosa, neglecting the exchange of the less soluble respiratory gases (i.e., oxygen and carbon dioxide). Heat and mass transfer coefficients are used to calculate the exchange rates of heat ($\dot{Q}_{\text{sens}}$) and mass ($\dot{n}_i$) between the mucosal surface and gas in the airway.

Figure 2 describes the airway mucosa in more detail. The entire mucosal tissue is treated as a dilute binary solution of soluble gas A in water with the physical properties of water. Diffusion of soluble gas A and water through the mucosa is assumed to be governed by Fick's law. The control of mucous hydration is simulated as follows: (a) the mucous thickness, ΔR_1, varies as liquid evaporates from or condenses

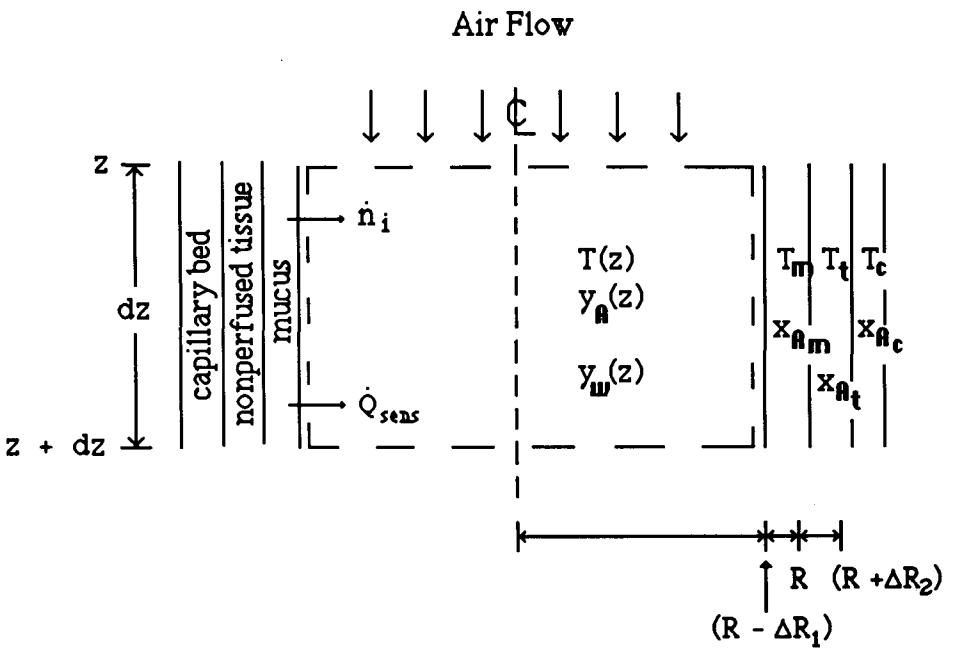

FIGURE 1. Control volume depiction of airway used to determine material and energy balances within any segment of the respiratory tract. The temperature and concentration variables shown represent bulk average values for each region: airway lumen, mucus of variable thickness ΔR_1, and nonperfused tissue layer of thickness ΔR_2.

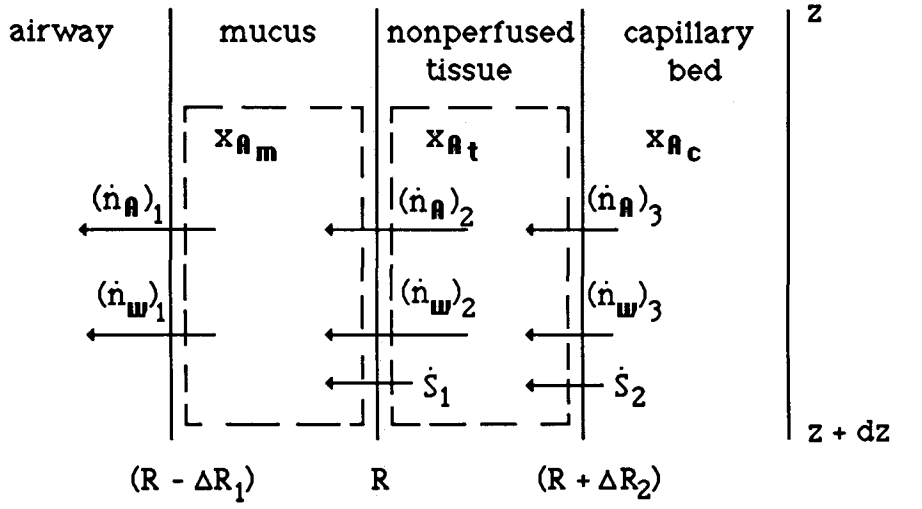

FIGURE 2. More detailed description of airway mucosa. Liquid lost from the mucus by evaporation is replenished by liquid secretion from the tissue, $\dot{S}_1$, and filtration from the capillaries, $\dot{S}_2$. Diffusion of water and soluble gas *A* through the mucosa is governed by Fick's law.

to the mucous surface, (b) reduction of the mucous thickness to a minimum value, $\Delta R_{\min}$, triggers the secretion of liquid from the nonperfused tissue to the mucus, preventing further dehydration; and (c) filtration of liquid from the capillaries maintains the nonperfused tissue hydration.

While the simulated changes in mucous thickness may seem somewhat artificial, they reflect the following aspects of the *in vivo* system. Mucus is a polyionic gel which contains two types of water, bound water in the gel matrix, and free water (23,28). Initially, the free water evaporates from the mucous gel. However, the much lower vapor pressure of the bound water makes it resistant to evaporation and, instead, further drying of the mucosal surface may stimulate secretion of more free water from the underlying tissue. The model assumes a simple relationship between mucous thickness and water content. However, a more complex function between mucous volume and water content may be included in future versions of the model. Incorporation of a variable mucous layer into the model allows the study of local hydration and dehydration of the mucus which may ultimately be significant to understanding how drying of the mucosal surface affects changes in local blood perfusion, stimulates mucus secretion, triggers bronchoconstriction, and affects acute and chronic dysfunctions of the mucociliary clearance.

Material and Energy Balances

The derivations of the energy and material balance equations are described in detail elsewhere (25). However, in this paper, the derivations will be outlined and the final forms of the equations presented.

The rate of accumulation of species i (either water or soluble gas, A) in the control volume depends on the net transport of i into and out of the control volume by convection of gas through the airway lumen, and by evaporation or condensation of species i from or to the airway mucosal surface. Using an order-of-magnitude analysis, Ingenito (12) demonstrated the axial diffusion of species i may be neglected. Assuming ideal gas law behavior, the total moles and total concentration in the control volume may be expressed in terms of the pressure and temperature of the control volume. Thus, the rate of accumulation of species i in the control volume may be written as follows:

$$\frac{\partial}{\partial t}\left[\frac{P_t A(z)dzy_i}{R(T+273.15)}\right] = \dot{V}\frac{\partial}{\partial z}\left[\frac{P_t y_i}{R(T+273.15)}\right]_z dz + \dot{n}_i \tag{1}$$

where P_t is the total pressure, $A(z)$ is the cross sectional area of the airway at z, R is the universal gas constant, y_i is the mole fraction of species i, T is the temperature in the control volume, $\dot{V}$ is the volumetric flow rate, and $\dot{n}_i$ is the molar evaporation rate of species i from the mucosal surface.

The molar flux may be expressed in terms of a local mass transfer coefficient and the mole fraction difference:

$$\dot{n}_i = P(z)dzk_{y_i}[y_{i,m} - y_i] \tag{2}$$

where $P(z)$ is the airway perimeter at z, k_{y_i} is the local mass transfer coefficient for i, and $y_{i,m}$ is the mole fraction of i at the mucosal surface.

The macroscopic energy balance written for the airway control volume is:

$$\left[\frac{\partial E_{\text{tot}}}{\partial t}\right]_{\text{c.v.}} = -\left[\frac{\partial(\dot{n}\tilde{H}^g)}{\partial z}\right]_z dz + \dot{Q}_{\text{sens}} + \sum_{i=1}^{2} \dot{n}_i \tilde{H}_i^g \tag{3}$$

where E_{tot} is the total energy in the control volume, $\dot{n}$ is the convective molar flow rate, $\tilde{H}^g$ is the enthalpy per mole of gas, $\dot{Q}_{\text{sens}}$ is the sensible heat transfer from the mucosal surface and $\tilde{H}_i^g$ is the enthalpy associated with the evaporation of species i from the mucosal surface. The sensible heat transfer rate may be expressed in terms of a local heat transfer coefficient:

$$\dot{Q}_{\text{sens}} = hP(z)dz(T_m - T) \tag{4}$$

where h is the local heat transfer coefficient, and T_m and T are the temperatures of the mucus and air, respectively. Neglecting the changes in potential and kinetic energy, the total energy E_{tot}, may be replaced with the internal energy, U_{tot}, which may be expressed in terms of the mole fractions and molar internal energies for each species, $\tilde{U}_i$. Specifying the reference state for the airway energy balance as all species in the gas phase at 0°C having zero enthalpy and assuming ideal gas behavior yield the following expression for the total internal energy in the control volume:

$$U_{\text{tot}} = \frac{P_t A(z)dz}{R(T + 273.15)} \sum_{i=1}^{3} y_i(\tilde{C}v_i T - 2270.0) \tag{5}$$

where $\tilde{C}v_i$ is the constant volume molar heat capacity for species i, -2270.0 is the reference state internal energy for each species (Note: $\tilde{U}_{\text{ref}} = \tilde{H}_{\text{ref}} - RT$). Similarly, by expressing the molar enthalpies in terms of the constant pressure molar heat capacities and by converting the molar flow rate to a volumetric flow rate using the ideal gas law, the final form of the energy balance in the airway may be derived from Eq. 3:

$$\frac{\partial}{\partial t}\left[\frac{P_t A(z)dz}{RT_{\text{abs}}} \sum_{i=1}^{3} y_i(\tilde{C}v_i T - 2270.0)\right] = -\frac{\partial}{\partial z}\left[\frac{P_t \dot{V}}{RT_{\text{abs}}} \sum_{i=1}^{3} y_i \tilde{C}p_i T\right]_z dz + \dot{Q}_{\text{sens}} + \sum_{i=1}^{2} \dot{n}_i \tilde{C}p_i T_m \tag{6}$$

where T_{abs} is the absolute temperature, $\tilde{C}p_i$ is the constant pressure heat capacity of species i, and all other terms are as previously defined.

The mass and energy balances in the mucosa are derived neglecting axial diffusion of soluble gas A and axial conduction of heat since these terms were shown to be negligible by Ingenito (12). Assuming that the mucus has the physical properties of water, the mucous thickness may be related to the moles of liquid in the control volume by a total molar balance:

$$\frac{\partial n_L}{\partial t} = \frac{P(z)dz\rho_w}{M_w} \frac{\partial \Delta R_1}{\partial t} = \dot{S}_1 - \sum_{i=1}^{2} (\dot{n}_i)_1 \tag{7}$$

where n_L is the moles of liquid in the mucous control volume, ρ_w is the density of water, M_w is the molecular weight of water, $\dot{S}_1$ is the rate of liquid secretion from the tissue to the mucus, and $(\dot{n}_i)_1$ is the molar flux rate of species i from the mucous surface defined by Eq. 2. The secretion rate depends on whether evaporation or condensation is occurring:

$$\text{If } \sum_{i=1}^{2} (\dot{n}_i)_1 < 0 \text{ then } \dot{S}_1 = 0$$

$$\text{If } \sum_{i=1}^{2} (\dot{n}_i)_1 > 0 \text{ and } \Delta R_1 > \Delta R_{\min} \text{ then } \dot{S}_1 = 0 \tag{8}$$

$$\text{otherwise } \dot{S}_1 = \sum_{i=1}^{2} (\dot{n}_i)_1 \ .$$

Since the moles of soluble gas A in the mucous control volume depend on the mucous thickness and mole fraction of A, the molar balance of A in the mucus may be written as follows:

$$\frac{\partial n_A}{\partial t} = \frac{\partial}{\partial t}\left[x_{Am} \frac{P(z)dz\Delta R_1 \rho_w}{M_W}\right] = (\dot{n}_A)_2 - (\dot{n}_A)_1 + \dot{S}_1 x_{At} \tag{9}$$

where n_A is the moles of A in the mucous control volume, x_{Am} and x_{At} are the mole fractions of A in the mucus and tissue, respectively, $(\dot{n}_A)_2$ is the diffusion rate of A from the tissue to the mucus and all other terms are as previously defined. The diffusion rate of A into the mucus is approximated using Fick's law as follows:

$$(\dot{n}_A)_2 = \frac{P(z)dz\rho_w D_{AW}}{M_W \frac{1}{2}(\Delta R_1 + \Delta R_2)} (x_{At} - x_{Am}) \tag{10}$$

where D_{AW} is the liquid phase diffusivity of A in water. The balance of soluble gas A in the nonperfused tissue is:

$$\frac{P(z)dz\rho_w \Delta R_2}{M_W} \frac{\partial x_{At}}{\partial t} = (\dot{n}_A)_3 - (\dot{n}_A)_2 + \dot{S}_2 x_{Ac} - \dot{S}_1 x_{At} \tag{11}$$

where $(\dot{n}_A)_3$ is the diffusive flow rate of A from the capillaries to the tissue, $\dot{S}_2$ is the filtration rate of liquid from the capillaries to the tissue, and x_{Ac} is the mole fraction of A in the capillaries. Assuming that the density and volume of the tissue are constant, the filtration rate $\dot{S}_2$ is equal to the secretion rate $\dot{S}_1$. The diffusive flow of A into the tissue, $(\dot{n}_A)_3$, is similar to that in Eq. 10:

$$(\dot{n}_A)_3 = \frac{P(z)dz\rho_w D_{AW}}{M_W \Delta R_2} (x_{Ac} - x_{At}) \ . \tag{12}$$

The energy balance in the mucus depends on the conductive and convective heat fluxes and the enthalpy transport associated with the molar fluxes:

$$\frac{P(z)dz\rho_w\tilde{C}p_w^l}{M_W}\left[\Delta R_1\frac{\partial T_m}{\partial t}+T_m\frac{\partial \Delta R_1}{\partial t}\right]=\dot{Q}_2-\dot{Q}_{\text{sens}}+\sum_{i=1}^{2}(\dot{n}_i)_2(\tilde{H}_i^l)_2-\sum_{i=1}^{2}(\dot{n}_i)_1(\tilde{H}_i^g)_1+\dot{S}_1\tilde{H}_1^l \tag{13}$$

where $\tilde{C}p_w^l$ is the molar heat capacity of liquid water, T_m is the mucous temperature, $\dot{Q}_2$ is the conductive heat transfer rate to the mucus, $\tilde{H}_i^l$ and $\tilde{H}_i^g$ are the molar enthalpies for species i in the liquid and gas phases, respectively, and all other terms are as previously defined. Assuming that the mucus has the thermal properties of water, the conductive heat transfer rate is approximated by Fourier's law:

$$\dot{Q}_2=\frac{P(z)dz(k_{th})_w}{\frac{1}{2}(\Delta R_1+\Delta R_2)}(T_t-T_m) \tag{14}$$

where $(k_{th})_w$ is the thermal conductivity of water and T_t is the tissue temperature. For the mucous energy balance, water, and soluble gas A in the liquid phase at 0°C will be the reference states. Thus, the molar enthalpy terms appearing in Eq. 13 are defined as follows:

$$\begin{aligned}(\tilde{H}_i^g)_1&=\Delta\tilde{H}_i^{\text{vap}}(0°\text{C})+\tilde{C}p_i^gT_m\\(\tilde{H}_i^l)_2&=\tilde{C}p_i^lT_m\\\tilde{H}_1^l&=[(1-x_{At})\tilde{C}p_w^l+x_{At}\tilde{C}p_A^l]T_t\end{aligned} \tag{15}$$

where $\Delta\tilde{H}_i^{\text{vap}}(0°\text{C})$ is the latent heat of vaporization for species i, and $\tilde{C}p_i^g$ and $\tilde{C}p_i^l$ are the molar heat capacities for species i in the gas and liquid phases, respectively.

Finally, the energy balance in the nonperfused tissue may be written as follows:

$$\frac{P(z)dz\rho_w\Delta R_2\tilde{C}p_w^l}{M_W}\frac{\partial T_t}{\partial t}=\dot{Q}_3-\dot{Q}_2+\sum_{i=1}^{2}[(\dot{n}_i\tilde{H}_i^l)_3-(\dot{n}_i\tilde{H}_i^l)_2]+\dot{S}_2\bar{H}_2^l-\dot{S}_1\tilde{H}_1^l \tag{16}$$

where $\dot{Q}_3$ is the conductive heat transfer rate between the capillaries and the tissue, and $\tilde{H}_2^l$ is the molar enthalpy of the filtrated fluid. The enthalpy terms are similar to those appearing in Eq. 15 and the rate of heat conduction from the capillaries to the tissue is given by:

$$\dot{Q}_3=\frac{P(z)dz(k_{th})_w}{\Delta R_2}(T_c-T_t) \tag{17}$$

where T_c is the capillary bed temperature.

Parameter Specification

Before the equations describing the dynamic heat and gas exchange processes occurring in the respiratory airways can be solved, several model parameters need to be specified. In order to provide maximal sensitivity in the analysis of soluble gas interactions with the airways, ethyl alcohol, which has the highest solubility of any gas exchanged by the lungs and for which data are easily found, was chosen as the soluble gas A for this study. Mean heat capacities for air, water vapor and alcohol, and heats of vaporization at 0°C were taken from Felder and Rousseau (6). Values for the Prandtl number, viscosity of air, density of water, thermal conductivities for air and water, and gas phase molecular diffusivities for alcohol and water in air at 37°C were obtained from Holman (10). The diffusivity of alcohol in water at infinite dilution was found in Reid, Sherwood, and Prausnitz (19).

Since the model equations were derived for a control volume in any airway segment, the entire respiratory tract may be modeled by dividing the nasal, oral, pharyngeal, tracheal, and bronchial passages into a series of compartments: 25 for oral breathing and 29 for nasal breathing. The average lengths and diameters of each compartment were taken from Hanna (7) for the upper airways and from Weibel (30) for the lower airways down to the 18th Weibel generation. The minimum mucous thickness, $\Delta R_{\min}$, was assumed to be 10μ in the first compartment and the ratio of the mucous thickness to the diameter of the compartment was maintained in subsequent compartments.

In the studies by Hanna (7), Ingenito (12), and Tsu (25), the capillary bed temperature profile, gas phase transfer coefficients, and nonperfused tissue thickness were identified as the model parameters having the largest effect on the model predictions. Thus, in this study, a range of values for each of these parameters was investigated. The tissue thickness, ΔR_2, was varied between .005 and .05 cm. Since Hanna assumed that the local blood temperature in the nasal or oral compartments, T_{head}, was 32°C or 34°C, respectively, which qualitatively agrees with the findings of Varene, Ferrus, Manier and Gire (27), the following capillary bed temperature profile was used: starting at T_{head} of either 32°C or 34°C in the nasal or oral compartments, T_c will rise linearly with axial distance to the mid-trachea, then level off at 37°C for all distal compartments. The effect of varying T_{head} on the model predictions was also examined. A more exact description of the airway mucosa requires more detailed information about the local blood flow, the local blood temperature, and the thermoregulatory and vascular responses to various stimuli. For example, the studies by several investigators (2,5,22) indicate that airway cooling occurs during hyperpnea of cold or dry air. Also, cold or dry air hyperpnea has been found to stimulate increased airway blood flow in response to reduced mucosal temperatures and airway drying (2). Full incorporation of airway perfusion into the model is complex and would probably involve some kind of feedback control mechanism which is beyond the scope of this study. Instead, the tissue thickness and capillary blood temperature profile parameters were chosen to characterize airway perfusion indirectly.

Different gas phase transfer coefficients were used in the model studies by Hanna (7) and Ingenito (12). Hanna measured mass transfer coefficients for the upper airway compartments using a naphthalene sublimation technique and derived analogous heat transfer coefficients. Ingenito measured heat transfer coefficients for the upper airways using a similitude technique and derived analogous mass transfer coefficients. Here, both sets of transfer coefficients will be used and the predicted results com-

pared. The correlation used by Hanna relating heat transfer coefficients to the Reynolds and Prandtl numbers has the following form:

$$Nu_{\phi,i} = \frac{hD}{(k_{th})_{\text{air}}} = C_{\phi,i} Re^{\alpha_{\phi,i}} Pr^{1/3} \tag{18}$$

where $Nu_{\phi,i}$ is the Nusselt number for phase of respiration (inspiration or expiration) ϕ and compartment i, $(k_{th})_{\text{air}}$ is the thermal conductivity of air, $C_{\phi,i}$ is a coefficient, Re is the Reynolds number, $\alpha_{\phi,i}$ is an exponent and Pr is the Prandtl number. The correlation used by Ingenito has the following form:

$$Nu_{\phi,i} = \frac{hD}{(k_{th})_{\text{air}}} = C_{\phi,i} (RePr)^{\alpha_{\phi,i}} . \tag{19}$$

Using the Chilton-Colburn analogy (24) and assuming ideal gas behavior, the mass transfer coefficient may be calculated from the heat transfer coefficient:

$$(k_y)_i = (1 - y_i)_M^{-1} \frac{h}{\tilde{C}_p} \left[\frac{\tilde{C}_p D_{i-\text{air}} P_t}{(k_{th})_{\text{air}} R T_{\text{abs}}} \right]^{2/3} \tag{20}$$

where $(1 - y_i)_M$ is the log-mean difference in the mole fraction of i, $\tilde{C}p$ is the molar heat capacity of the mixture, $D_{i-\text{air}}$ is the binary gas phase diffusivity of species i in air, and all other terms are as previously defined.

Boundary Conditions

At the airway-mucus interface, equilibrium between the gas and liquid is assumed. Assuming that Raoult's law holds for water, the gas phase mole fraction of water at the air/mucus interface, $(y_w)_m$, may be calculated from the saturation vapor pressure of water given by the Antoine equation (6) and the liquid phase mole fraction, $(x_w)_m$. For a very dilute solution of ethanol in water, the following vapor-liquid equilibrium expression holds:

$$(y_A)_m = \frac{R(T_m + 273.15)}{P_t} \frac{\rho_w}{M_W} \frac{x_{Am}}{\lambda(T_m)} \tag{21}$$

where $\lambda(T_m)$ is the partition coefficient defined as the ratio of the concentration of alcohol in the liquid phase to the concentration in the gas phase. Jones' correlation for the partition coefficient as a function of temperature for the alcohol/water/air system is used (14). The capillary blood alcohol mole fraction, $(x_A)_c$, assumed constant along the entire airway tract, is calculated from a specified blood alcohol concentration, BAC.

During inspiration, the inlet conditions at the proximal end of the airway will correspond to those of the ambient air. The concentration of alcohol in the inspired gas is assumed to be zero. During expiration, the model assumes that the alveolar gas entering the distal end of the airway is at body temperature, fully saturated with water and equilibrated with the blood alcohol. The volumetric flow rate is a sinusoidal function of time. Initially, at $t = 0$, all eight variables, T, T_m, T_t, y_A, y_w, $(x_A)_m$,

$(x_w)_t$, and ΔR_1, are functions of axial position. These functions are chosen by the user for the very first simulation, but are provided by preceding simulations for succeeding ones.

Numerical Solution Methods

The mathematical model described by Eqs. 1 through 17 consists of eight hyperbolic differential equations which must be solved simultaneously for each axial position, z, and time, t. If the length of each compartment is divided into N control volumes, the resulting system would require simultaneous solution of $(8 \times N)$ equations for every iteration. This enormous task can be handled only by a numerical solution scheme solved on a computer.

First, the variables are nondimensionalized and normalized to allow for both more accurate and more efficient numerical solution. The spatial derivatives are described by upstream finite differencing. Let the subscript j on any term designate the value of that term at the jth grid point. Thus, for any function χ the z-derivative is:

$$\frac{\partial \chi}{\partial z} = \frac{\chi_j - \chi_{j-1}}{\Delta z} . \tag{22}$$

Numerical integration of the time derivatives is handled using LSODE, a time-integration software package developed by Hindmarsh (9) which solves systems of differential equations of the following form:

$$\frac{\partial y_i}{\partial t} = f_i(y_1, y_2, \ldots, y_n) \quad i = 1,2,\ldots,n . \tag{23}$$

There are several advantages to using LSODE: (a) the user need not develop his own algorithm, (b) an implicit integration scheme is employed for greater accuracy, (c) error tolerances are specified by the user, (d) a variable time step is used, and (e) problems with steep gradients, are handled easily.

The Alcohol Elimination Simulator consists of three FORTRAN programs written by Tsu (25), CREATE, ETOH, and FEX, which are linked with the LSODE packaged subroutine. CREATE is an interactive program which creates the first input data file. ETOH, the main program in the Alcohol Elimination Simulator, solves the system of hyperbolic differential equations for one complete phase of inspiration or expiration and creates an output file. FEX, a subroutine called by LSODE, calculates the time derivative of each variable. Compiled versions of ETOH, FEX, and LSODE are linked to form an executable program which is submitted as a batch job for the simulation of each breathing phase to a VAX computer.

RESULTS AND DISCUSSION

Simulations

Before the model predictions can be interpreted with any confidence, the simulated results need to be compared to *in vivo* experimental data. For oral breathing, McFadden *et al.* (17) measured the end-inspiratory and end-expiratory airway temperature profiles between the trachea and the subsegmental bronchus using a multiple

thermistor probe for several levels of ventilation. For nasal breathing, Hanna and Scherer (8) compiled airway temperature and water concentration data from several sources. Thus, for purposes of comparison, the conditions used in the oral breathing simulations were the same as those of the McFadden experiments: $\dot{V}_E = 15$ l/min ($f = 15$ min^{-1} and $V_T = 1.0$ liter); $T_{amb} = 26.7$°C; and $RH = 34.8\%$. Similarly, the nasal breathing simulations were made using the conditions assumed by Hanna: $\dot{V}_{ave} = 300$ ml/sec ($f = 12$ min^{-1} and $V_T = 750$ ml); $T_{amb} = 23.0$°C; and $RH = 30.0\%$.

In order to choose the set of model parameters that gives the best fit with the data and to analyze the sensitivity of the predictions to changes in the parameters, the factorial design method (1) was used to design each "experiment" or simulation. Table 1 describes the lower and upper values of each parameter used in each simulation in the 2^3 full factorial design (there are 2 levels for each of the 3 parameters). Each simulation consisted of either three breaths or six breaths for ΔR_2 equal to .005 cm or .05 cm, respectively, since the thinner tissue thickness required fewer breaths to reach periodic steady state conditions. The set of eight simulations was executed twice, once for oral breathing and again for nasal breathing. Calculated with Yates' algorithm (1), the main effect of each parameter for several responses of interest are shown in Table 2.

Model Predictions vs. Experimental Data—Oral Breathing

Since the model uses average lengths of airways determined by Hanna (7) and Weibel (30), the axial positions measured by McFadden *et al.* were adjusted to match various anatomical landmarks. Comparison between the measured and predicted end-inspiratory and end-expiratory temperatures was poor for all simulations and the set of parameters giving the best fit for the inspiratory data gave the worst fit for the expiratory data and vice versa. This result, however, may be attributed to the slow

TABLE 1. Parameter values used in each simulation of the 2^3 factorial design.

		Model Parameters		
	Level	T_{head}(°C)	ΔR_2 (cm)	$h(z)$
	Lower Level (−)	34.0–oral (32.0–nasal)	.005	Hanna
	Upper Level (+)	37.0	.05	Ingenito
Simulation				
1		−	−	−
2		+	−	−
3		−	+	−
4		+	+	−
5		−	−	+
6		+	−	+
7		−	+	+
8		+	+	+

TABLE 2. Sensitivity of simulated responses to changes in model parameters, calculated average values, and main effects.

		Model Parameters					
		T_{head} (°C)		ΔR_2 (cm)		$h(z)$	
Responses	Average	34.0	37.0	.005	.05	Hanna	Ingenito
1. $\Sigma (T_p - T_d)^2$ oral breathing	7.15	5.44	8.86	10.77	3.53	12.69	1.61
2. T_{min} – air (°C) (carina)	33.4	33.2	33.6	34.1	32.7	34.6	32.2
3. T_{ave} – mucus (°C) (prox. trachea)	35.7	35.0	36.4	36.1	35.3	35.9	35.5
4. T_{ave} – tissue (°C) (prox. trachea)	35.9	35.2	36.6	36.2	35.6	36.0	35.8
5. Water Loss (g/min)	.487	.479	.495	.492	.482	.491	.483
6. Heat Loss (J/min)	1706	1683	1730	1720	1693	1718	1695
7. % Increase ΔR_1 (prox. trachea)	.78	1.38	.19	.65	.92	.20	1.36
8. (ave x_A)/x_{Ac} – mucus (prox. trachea)	.796	.805	.786	.885	.706	.812	.780
9. (ave x_A)/x_{Ac} – tissue (prox. trachea)	.905	.909	.901	.929	.882	.922	.889
10. $\Sigma (T_p - T_d)^2$ nasal breathing	25.2	11.5	39.0	33.4	17.1	26.6	23.9

response time of the thermistors. McFadden *et al.* (17) reported a 63% response time of .250 seconds for the thermistors in a stirred water bath. However, the heat transfer coefficient for the thermistor in air is much less than it would be in water, and thus, the response time of the thermistor in air must be much longer than that for water (4). Consequently, the experimental data cannot be an accurate reflection of the instantaneous temperatures predicted by the model; the slow response time causes the measured minimum and maximum airway temperatures to be attenuated relative to the actual values. While the amplitude of the measured cyclical changes in airway temperature may be reduced, the mean airway temperatures measured by the thermistors should be identical to the actual mean values. Thus, a more appropriate criterion for best fit of the model predictions to the experimental data may be some mean or average airway temperature. Two alternative mean temperatures can be used: (a) the integrated time average temperature over the entire inspiratory and expiratory phases, $(T_{ave})_1$, and (b) the arithmetic mean of the minimum inspiratory and maximum expiratory temperatures, $(T_{ave})_2$. Since the sum-of-squared-error using $(T_{ave})_2$ was less than that using $(T_{ave})_1$ for every simulation, a comparison between $(T_{ave})_2$ and the arithmetic mean of the measured end-inspiratory and end-expiratory temperatures was used as the criterion for best fit.

The first row in Table 2 gives the average sum-of-squared-error, $\Sigma(T_p - T_d)^2$ where T_p is $(T_{ave})_2$ and T_d is the mean of the measured inspiratory and expiratory temperatures, for all simulations and the effects of changing the model parameters. The choice of heat transfer coefficient, $h(z)$, had the most significant effect on the fit; using Ingenito's coefficients rather than Hanna's reduced the $\Sigma(T_p - T_d)^2$ from 12.69 to 1.61. The next most significant parameter was the nonperfused tissue thickness, ΔR_2, and the capillary bed temperature in the head, T_{head}, affected the error the least; decreasing T_{head} or increasing ΔR_2 decreased the error. Thus, the set of parameters giving the best fit between the predicted and measured mean airway temperatures is: $T_{head} = 34°C$; $\Delta R_2 = .05$ cm; and Ingenito's heat transfer coefficients. These parameters will be referred to as the base case parameters for the remainder of this paper.

Figure 3 shows the comparison between the predicted and measured airway temperatures for the base case parameters. The arithmetic mean, $(T_{ave})_2$, fits the data better than the integrated average, $(T_{ave})_1$. The predicted airway temperature fluctuations are attenuated in differing degrees by the various thermistors suggesting that the thermistor response is nonlinear in addition to being slow. During inspiration, the inspired air is essentially completely conditioned by the 10^{th} generation. During expiration, the air experiences the greatest amount of cooling in the oral and pharyngeal regions. The average expiratory temperature at the mouth is 34.8°C which is 1.6°C cooler than the predicted end-expiratory temperature.

Conditioning Efficiency

The average minimum air temperature at the carina for all simulations is 33.4°C (see Table 2) which is affected most significantly by changes in $h(z)$. Using Ingenito's coefficients, reducing T_{head} and increasing ΔR_2, reduces T_{min} at the carina and, hence, reduces the conditioning efficiency of the extrathoracic airways. Figure 4 shows the effects of changing the model parameters on the minimum relative humidity profile in the airway. Using Hanna's heat transfer coefficients rather than

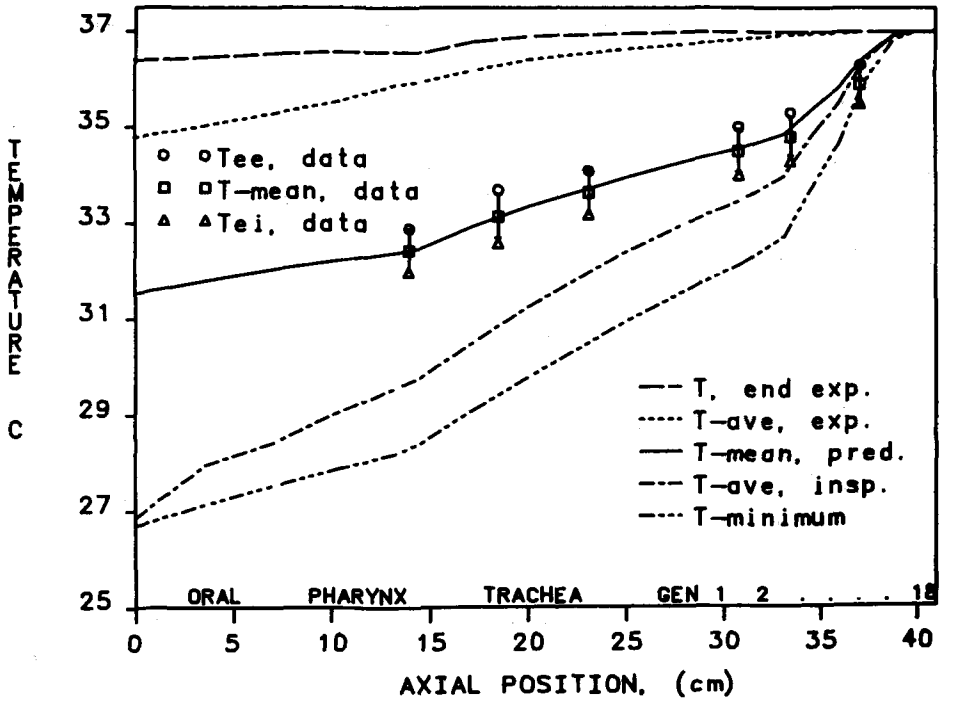

FIGURE 3. Comparison of predicted end-expiratory, end-inspiratory, and average airway temperature profiles with literature data for quiet, oral breathing of room air using base case model parameters (see text). While the measured minimum and maximum airway temperatures are greatly attenuated relative to the predicted values, the mean airway temperature profile agrees well with the predicted averages.

Ingenito's dramatically increases the relative humidity of the inspired air beyond the oropharynx. Hanna assumed that the heat transfer coefficient function in the oropharynx during oral breathing is approximately seven times what it is during nasal breathing because of the sharp change in the direction of the airflow in the oropharynx during oral breathing. This assumption results in the dramatic differences observed between the model predictions using Hanna's coefficients and Ingenito's coefficients. Thus, during oral breathing of room air at rest, the greatest amount of conditioning of the inspired air occurs in the trachea and larger bronchi, the smaller bronchial airways participate in the conditioning process, and the inspired air is not fully conditioned until the 10^{th} generation.

Conservation of Water and Heat

The respiratory water loss (RWL) and respiratory heat loss (RHL) were calculated by numerically integrating over one breath the amount of water in the air and the enthalpy of the air, respectively, at the mouth. The average RWL and RHL for all simulations are .487 g/min and 1706 J/min, respectively (see Table 2). Changing the capillary bed temperature in the head, T_{head}, had the most significant effect on the water and heat losses; increasing T_{head} from 34.0°C to 37.0°C increased the RWL from .479 to .495 g/min and increased the RHL from 1683 to 1730 J/min. The pre-

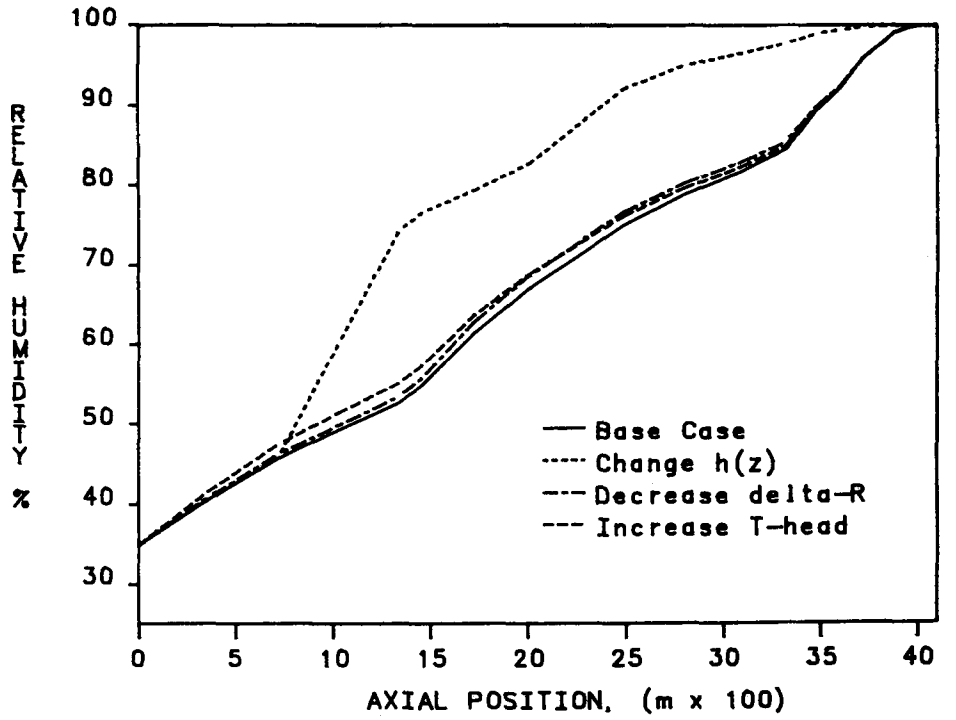

FIGURE 4. Predicted minimum relative humidity profiles in the airway during inspiration for the base case model parameters and the effects of changing (a) the heat transfer coefficient correlation, (b) the nonperfused tissue thickness, and (c) the capillary bed temperature in the head. Deeper penetration of unconditioned air is predicted by the model when Ingenito's coefficients are used instead of Hanna's.

dicted losses were also increased by decreasing the nonperfused tissue thickness and using Hanna's transfer coefficients. Reduction of the RWL and RHL largely depends on the ability of the airways to recover water and heat lost during inspiration from the expired air. Cooling of the airway mucosal surface due to the sensible and evaporative heat losses enhances the recovery of water and heat.

Thus, a tradeoff exists between conditioning efficiency and body heat and water conservation. A thicker mucosal tissue better insulates the airway surface from the capillary bed resulting in greater cooling of the surfaces, reduced conditioning efficiency and greater penetration of unconditioned air, but increased heat and water recovery. A cooler steady-state capillary bed temperature reduces the conditioning efficiency causing deeper penetration of unconditioned air, but increases the recovery of heat and water from the expired air. In the absence of better information pertaining to the perfusion characteristics of the airway tissue, a study of how the model parameters affect the predicted heat and water losses has revealed the following: the model parameters giving the best fit between the model predictions and *in vivo* experimental data, namely $T_{head} = 34°C$, $\Delta R_2 = .05$ cm, and Ingenito's coefficients, are also the model parameters predicting the lowest RWL and RHL, the greatest percent heat recovery, but the poorest conditioning efficiency. This suggests that for the oral,

quiet breathing of room air, the conservation of body heat and water may be more important than the efficient conditioning of the inspired air.

Figure 5 shows the heat flux from the mucosal surface at the mouth as a function of time for one complete breath. The total heat flux consists of two components, the sensible heat flux due to the temperature gradient and the latent heat flux due to the evaporation and condensation of water and alcohol. The latent heat transfer comprises 92% and 83% of the total heat transferred during inspiration and expiration, respectively. The heat flux from the mucosal surface is maximum during mid-inspiration when the volumetric flow rate is greatest. The surface continues to lose heat during the early part of expiration while the incompletely conditioned dead space volume of air is being eliminated. The sensible and latent heat fluxes are negative for the rest of expiration, demonstrating the transfer of heat and condensation of liquid from the expired air to the cooler airway surface. The heat recovered during expiration is only 8.0% of that lost during inspiration, and thus there is a net loss of heat from this point during each breath.

Changes in Mucous Thickness

The average for all simulations of the maximal percent increase in the mucous thickness in the proximal trachea is .78% (see row 7 in Table 2). The capillary bed

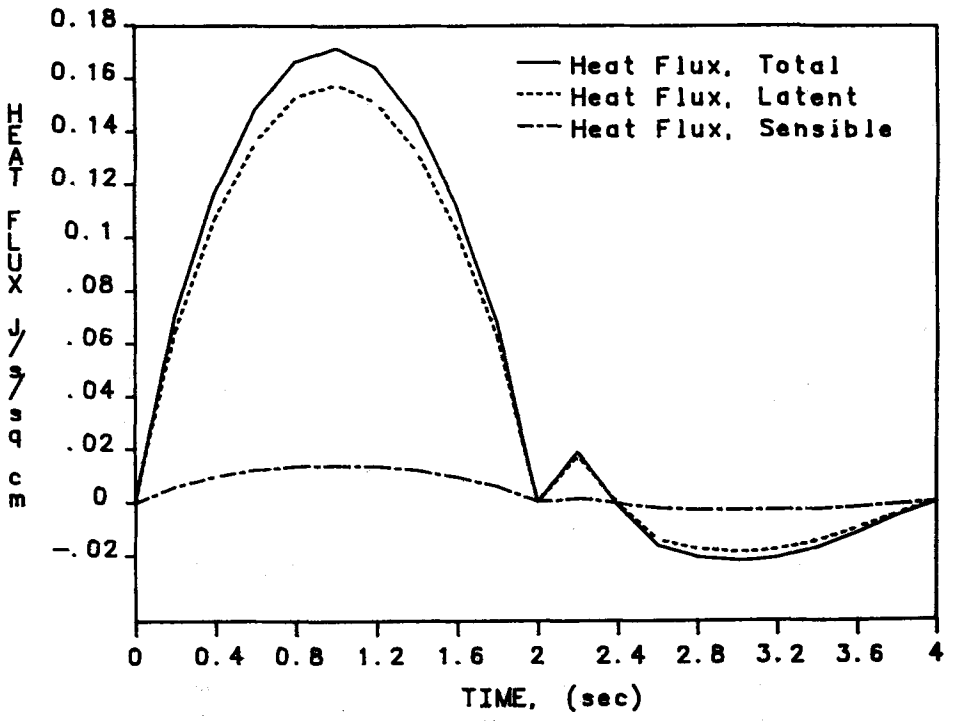

FIGURE 5. Base case predictions of the total heat flux and the sensible and latent component heat fluxes from the mucous surface to the air at the mouth entrance as a function of time for one complete breath. The sensible heat flux is that due to the temperature gradient and the latent heat flux is that due to the evaporation and condensation of water and alcohol.

temperature in the head, T_{head}, affected the increase in the mucous thickness the most; the mucous thickness increased by 1.38% for T_{head} equal to 34°C but only increased by .19% for T_{head} equal to 37°C. The predicted percent increase in the mucous thickness was greater when Ingenito's transfer coefficients were used and when ΔR_2 was increased. Thus, a cooler capillary bed temperature, a thicker non-perfused tissue layer, and higher heat transfer coefficients increase the local heat transfer from the mucous surface, resulting in lower mucous temperatures, greater condensation of liquid during expiration, and greater swelling of the mucous layer.

Figure 6 shows the predicted dynamic changes in the mucous layer for several axial positions using the base case model parameters. For all positions, evaporation during inspiration causes a rapid decrease in the layer thickness down to the controlled minimum mucous layer thickness, ΔR_{min}. During the rest of inspiration and the early part of expiration, liquid lost by further evaporation is compensated by the simulated secretion of liquid from the tissue and no change in the mucous thickness occurs. During expiration, condensation of liquid from the expired air to the cooler mucous surface causes the mucous layer to swell. Evaporation during inspiration occurs sooner in the proximal airways than in the distal airways while condensation occurs sooner in the distal airways than in the proximal ones, reflecting the transport

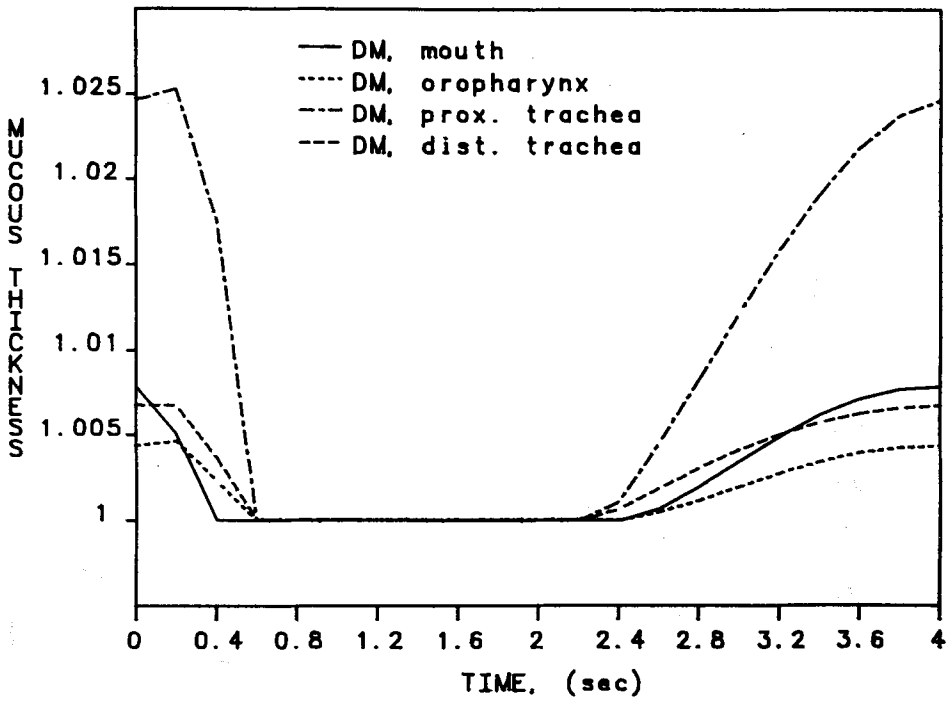

FIGURE 6. The predicted mucous layer thickness normalized with respect to the minimum controlled thickness, ΔR_{min}, as a function of time during one complete breath at various locations in the respiratory tract. The mucous thickness is quickly reduced by evaporation to the minimum level where it is maintained by simulated fluid secretion from the tissue during inspiration. Condensation of liquid from the expired air to the cooler mucosal surface causes the mucus to thicken during expiration.

time of the flowing air between the various positions in the airway. The mucus in the proximal trachea experiences the greatest amount of swelling relative to that in the mouth, oropharynx, and distal trachea.

Alcohol Interactions with the Airway Mucosa

For the proximal trachea, the average alcohol mole fractions normalized with respect to the mole fraction of alcohol in the capillary bed, $\langle x_A \rangle / x_{Ac}$, in the mucus and nonperfused tissue are .796 and .905, respectively (see rows 8 and 9 in Table 2). Thus, the airway mucosa is relatively stripped of alcohol and represents a sink for alcohol both from the capillaries and from the expired air. The nonperfused tissue layer had the largest impact on the alcohol mole fraction; increasing ΔR_2 decreases $\langle x_A \rangle / x_{Ac}$ in both the mucus and tissue by decreasing the diffusion rate of alcohol through the airway mucosa. Increasing T_{head} also decreases $\langle x_A \rangle / x_{Ac}$ by reducing the solubility of alcohol in the warmer airway mucosa. Since the model predicts higher heat and mass transfer rates in the proximal trachea using Ingenito's coefficients, the predicted $\langle x_A \rangle / x_{Ac}$ in the mucus and tissue of the proximal trachea is lower when Ingenito's coefficients are used.

Figure 7 describes the partial pressure of alcohol, P_A, normalized with respect to the alveolar partial pressure, as a function of time for the air, mucus, and tissue at

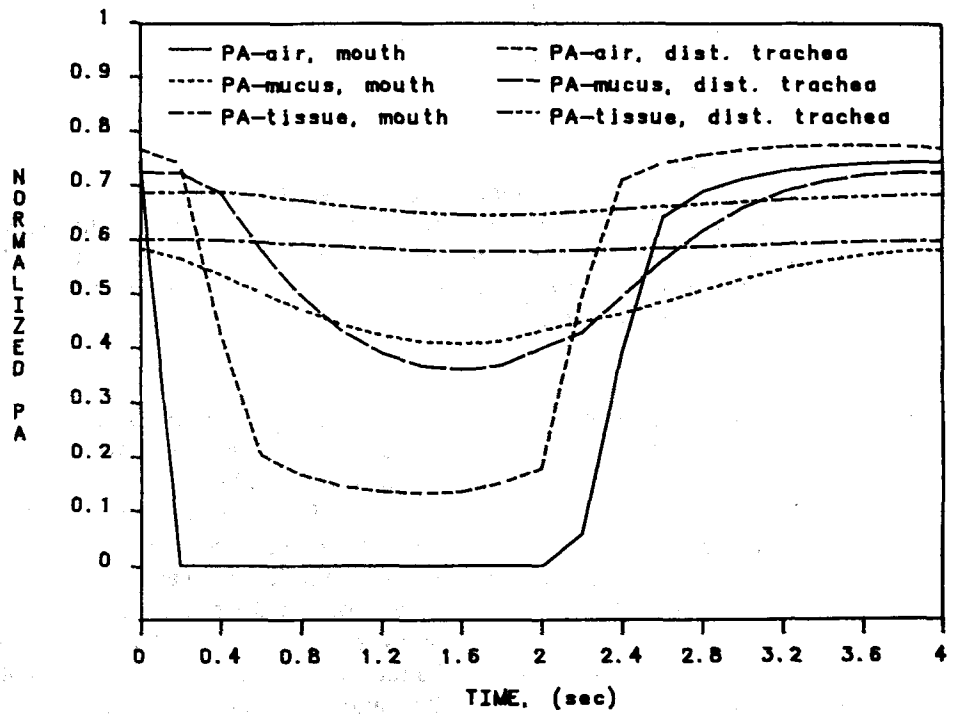

FIGURE 7. Base case predictions of the alcohol partial pressure, normalized with respect to the alveolar level, as a function of time for one breath in the air, mucus, and tissue in the mouth and distal trachea.

the mouth and distal end of the trachea. The partial pressures in the mucus and tissue were calculated using Eq. 21. Periodic fluctuations in P_A occur in all three regions of the airway with the amplitude of the fluctuations decreasing from the air to the mucus to the tissue. The relative magnitude of the P_A in the air to the P_A in the mucus determines the direction of alcohol transport; when the P_A in the air is less than that in the mucus, alcohol is stripped from the mucus while absorption of alcohol by the mucus from the air occurs when the situation is reversed. In any given region, the P_A increases with increasing distance from the mouth. Because of the absorption of alcohol by the mucus from the expired air along the entire airway, the final P_A at the mouth is only 74.5% of the alveolar level. Thus, during tidal breathing of room air, the final P_A measured at the mouth is not an accurate measurement of the alveolar P_A.

Nasal Breathing

Assuming that the temperature sensing devices had a relatively slow response time, the airway temperature data compiled by Hanna for nasal breathing more accurately reflects the mean rather than the inspiratory airway temperatures. Thus, the comparison between the predicted and measured mean airway temperatures will again be used as the criterion for degree of fit. The average sum of squared error, $\Sigma(T_p - T_d)^2$, for all nasal breathing simulations is 25.2 (see Table 2, row 10). Decreasing T_{head}, increasing ΔR_2, and using Hanna's transfer coefficients decreases the $\Sigma(T_p - T_d)^2$. Thus, for nasal breathing, the base case model parameters giving the best fit are: $T_{\text{head}} = 32.0°\text{C}$, $\Delta R_2 = .05$ cm, and Hanna's transfer coefficients. Figure 8 shows the comparison between the literature data and the predicted airway temperatures using the base case parameters. The integrated average, $(T_{\text{ave}})_1$, and the arithmetic mean, $(T_{\text{ave}})_2$, give a similar fit with the average airway temperature data. The average temperature of the inspired air increases steadily, reaching body core temperature by the 6$^{\text{th}}$ generation. The average temperature of the expired air at the nose is 33.9°C while the end-expired temperature is 34.9°C. As for oral breathing, the cooling of the expired air in the upper respiratory airways is caused by the recovery of heat and water by the cooler mucosal surfaces and serves to minimize the RWL and RHL from the body. For nasal breathing, the base case predicted RWL and RHL are .298 g/min and 1002 J/min, respectively.

Hyperpnea of Room Air

Since part of the utility of the computer model rests in its ability to predict the dynamic physiological events at other conditions, the model was used to simulate hyperpnea of room air. Two additional simulations were made at ventilation rates of 30 l/min and 60 l/min with $T_{\text{amb}} = 26.7°\text{C}$; and $RH = 34.8\%$ and compared to the data reported by McFadden *et al.* (17). Since one would expect the steady-state capillary bed temperature profile to decrease as ventilation increases, the model parameter T_{head} was adjusted until the best fit was obtained while all other model parameters remained unchanged. Figure 9 shows the comparison between the predicted average airway temperatures and McFadden's data for $\dot{V}_E = 15$, 30, and 60 l/min. The values of T_{head} used are 34°C, 32°C, and 30°C, corresponding to $\dot{V}_E =$ 15, 30, and 60 l/min. Thus, in order to maximize the model's predictive value, the capillary bed temperature profile must be known as a function of inspired air conditions and ventilation rate.

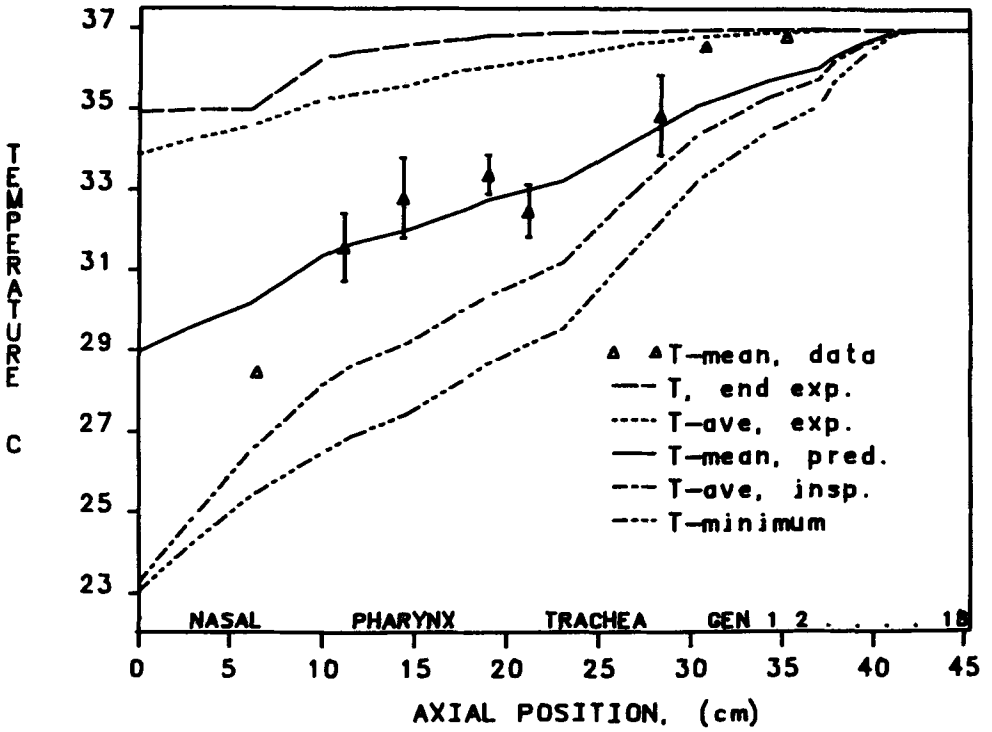

FIGURE 8. Comparison of mean airway temperature data from the literature for nasal breathing with base case model preditions of the average, end-expiratory, and minimum-inspiratory airway temperature profiles. See text for definitions of $(T_{ave})_1$ and $(T_{ave})_2$.

CONCLUSIONS

A one dimensional theoretical model describing the heat and water exchange processes occurring in the respiratory airways has been extended to include the exchange of a soluble gas with the airway mucosa, the change in the mucous layer thickness due to evaporation and condensation of water during respiration, and the secretion and filtration of liquid from the tissue and capillary bed, respectively, to maintain mucosal tissue hydration. The predicted mean airway temperature profiles agreed well with *in vivo* experimental data taken from the literature for both oral and nasal breathing. Using Ingenito's heat transfer coefficient correlations gave a better fit for oral breathing while Hanna's correlations gave a better fit for nasal breathing. For both oral and nasal breathing, decreasing the capillary bed temperature in the head and increasing the thickness of the nonperfused tissue improved the degree of fit with the experimental data and resulted in a set of model parameters that also increased the heat recovery in the upper respiratory airways and minimized the respiratory heat and water losses from the body. For the quiet breathing of room air, the conservation of heat and water may be more important than the conditioning efficiency of the airways, since the inspired air continues to be conditioned within the larger bronchial airways and is not fully conditioned until the 10^{th} and 6^{th} generations for oral and nasal breathing, respectively. The model parameters maximizing the heat and

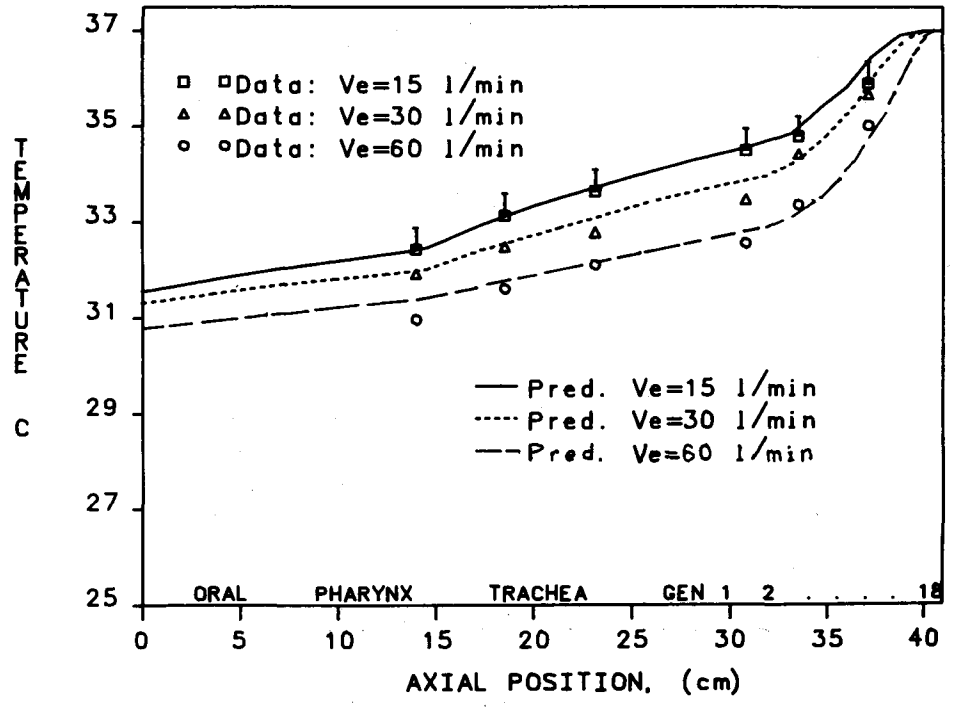

FIGURE 9. Comparison of simulated mean airway temperatures with literature data for ventilation rates of 15, 30, and 60 l/min with T_{head} = 34°C, 32°C, and 30°C, respectively.

water recovery in the airways predicted the lowest average mucous temperatures and the greatest increases in the mucous thickness due to the condensation of liquid to the cooler mucosal surface during expiration. For the quiet, tidal breathing of room air through the mouth, the model predicts a final expired partial pressure of alcohol that is only 74.5% of the alveolar level due to the absorption of alcohol from the expired air by the airway mucosa during exhalation. In future studies, the model will be used to compare oral and nasal breathing of dry room air, analyze the effects of large changes in inspired air conditions and breathing pattern, simulate the interactions of alcohol with the airway mucosa during a prolonged exhalation, and simulate the dynamic uptake of inhaled toxic gases by the airway mucosa. Improvement of the model requires a better understanding of the nature of the airway mucosa, specifically, the physical chemistry and secretion mechanism of the mucus, the thickness of the nonperfused tissue layer, the temperature of the capillary bed and the changes in the perfusion of the mucosa in response to drying and cooling of the tissue.

REFERENCES

1. Box, G.E.P.; Hunter, W.G.; Hunter, J.S. Statistics for experimenters, New York: John Wiley & Sons; 1978.
2. Baile, E.M.; Dahlby, R.W.; Wiggs, B.R.; Parsons, G.H.; Pare, P.E. Effect of cold and warm dry air hyperventilation on canine airway blood flow. J. Appl. Physiol., 62:526-532; 1987.

3. Cole, P. Further observations on conditioning of respiratory air. J. Laryngol. Otol., 67:669–681; 1953.
4. Coughanowr, D.R.; Koppel, L.B. Process systems analysis and control. New York: McGraw-Hill; 1965.
5. Deal, E.C., Jr.; McFadden, E.R., Jr.; Ingram, R.H., Jr.; Jaeger, J.J. Esophageal temperature during exercise in asthmatic and nonasthmatic subjects. J. Appl. Physiol., 46:484–490; 1979.
6. Felder, R.M.; Rousseau, R.W. Elementary principles of chemical processes. New York: John Wiley & Sons; 1978.
7. Hanna, L.M. Modelling of heat and water vapor transport in the human respiratory tract (Ph.D. diss.), Philadelphia, University of Pennsylvania; 1983.
8. Hanna, L.M.; Scherer, P.W. Regional control of local airway heat and water vapor losses. J. Appl. Physiol., 61:624–632; 1986.
9. Hindmarsh, A. LSODE, (computer program). Lawrence Livermore Laboratory; 1981.
10. Holman, J.P. Heat transfer, 5th ed. New York: McGraw-Hill; 1981.
11. Ingelstedt, S. Studies on conditioning of air in the respiratory tract. Acta Otolaryngol. Suppl. 131:1–80, 1956.
12. Ingenito, E.P. Respiratory fluid mechanics and heat transfer (Ph.D. diss.), Cambridge, Massachusetts Institute of Technology; 1984.
13. Ingenito, E.P.; Solway, J.; McFadden, E.R., Jr.; Pichurko, B.M.; Cravalho, E.G.; Drazen, J.M. Finite difference analysis of respiratory heat transfer. J. Appl. Physiol. 61:2252–2259; 1986.
14. Jones, A.W. Determination of liquid/air partition coefficients for dilute solutions of ethanol in water, whole blood, and plasma. J. Analytical Toxicology. 7:193–197; 1983.
15. Kruse, K.L. Heat and water transport dynamics in the respiratory tract (M.S. thesis). Cleveland, Case Western Reserve University; 1981.
16. McEvoy, R.D.; Davies, N.J.H.; Mannino, F.L.; Prutow, R.J.; Schumacker, P.T.; Wagner, P.D.; West, J.B. Pulmonary gas exchange during high-frequency ventilation. J. Appl. Physiol.: Respirat. Environ. Exercise Physiol. 52:1278–1287; 1982.
17. McFadden, E.R.; Pichurko, B.M.; Bowman, H.F.; Ingenito, E.; Burno, S.; Dowling, N.; Solway, J. Thermal mapping of the airways in humans, airway temperature during respiration. J. Appl. Physiol. 58:564–570; 1985.
18. Netter, F.H. The CIBA collection of medical illustrations, vol. 7, respiratory system. Summit, NJ: Ciba Pharmaceutical Company; 1979.
19. Reid, R.C.; Sherwood, T.K.; Prausnitz, J.M. The properties of gases and liquids, 3rd ed. New York: McGraw-Hill; 1980.
20. Robertson, H.T.; Coffey, R.L.; Standaert, T.A.; Truog, W.E. Respiratory and inert gas exchange during high-frequency ventilation. J. Appl. Physiol.: Respirat. Environ. Exercise Physiol. 52:683–689; 1982.
21. Saidel, G.M.; Kruse, K.L.; Primiano, F.P., Jr. Model simulation of heat and water transport dynamics in an airway. J. Biomech. Eng. 105:189–193; 1983.
22. Solway, J.; Pichurko, B.M.; Ingenito, E.P.; McFadden, E.R., Jr.; Fanta, C.H.; Ingram, R.H., Jr.; Drazen, J.M. Breathing pattern affects airway wall temperature during cold air hyperpnea in humans. Am. Rev. Respir. Dis. 132:853–857; 1985.
23. Tam, P.Y.; Verdugo, P. Control of mucus hydration as a donnan equilibrium process. Nature, 292:340–342; 1981.
24. Treybal, R.E. Mass transfer operations. New York: McGraw-Hill; 1980.
25. Tsu, M.E. Mathematical and experimental modeling of heat, water, and soluble exchange in the trachea (M.S. thesis), Seattle, University of Washington; 1986.
26. Vander, A.J.; Sherman, J.H.; Luciano, D.S. Human physiology: mechanisms of body function. New York: McGraw-Hill; 1985.
27. Varene, P.; Ferrus, L.; Manier, G.; Gire, J. Heat and water respiratory exchange comparison between mouth and nose breathing in humans. Clinical Physiol., 6:405–414, 1986.
28. Verdugo, P. Hydration kinetics of exocytosed mucins in cultured secretory cells of the rabbit trachea: a new model. In: Nugent, J.; O'Conne, M., eds. Mucus and mucosa. London: Pittman; 1984, pp. 212–225.
29. Wagner, P.D., Saltzman, H.A.; West, J.B. Measurement of continuous distribution of ventilation-perfusion ratio: theory. J. Appl. Physiol. 36:588–599; 1974.
30. Weibel, E. Morphometry of the human lung. New York: Springer-Verlag; 1963.

NOMENCLATURE

$A(z)$ = airway cross sectional area, cm^2
$\alpha_{\phi,i}$ = exponent in Nusselt number correlation
BAC = blood alcohol concentration
$C_{\phi,i}$ = coefficient in Nusselt number correlation
$\tilde{C}p_i^g$ = gas phase constant pressure molar heat capacity, J/(°C mol i)
$\tilde{C}p$ = constant pressure molar heat capacity of gas mixture, J/(°C mol i)
$\tilde{C}p_i^l$ = liquid phase constant pressure molar heat capacity, J/(°C mol)
$\tilde{C}v_i$ = constant volume molar heat capacity for species i, J/(°C mol i)
D = airway diameter, cm
D_{AW} = liquid phase diffusivity of A in water, cm^2/s
$D_{i-\text{air}}$ = binary gas phase diffusivity of species i in air, cm^2/s
E_{tot} = total energy in airway control volume, J
f = breathing frequency, breaths/s
$h, h(z)$ = local heat transfer coefficient, J/(cm^2 s°C)
$\Delta\tilde{H}_i^{\text{vap}}$ = latent heat of vaporization for species i, J/(mol i)
$\tilde{H}^g$ = gas phase molar enthalpy, J/mol
$\tilde{H}_2^l$ = molar enthalpy of filtrated fluid, J/mol
$\tilde{H}_i^g, \tilde{H}_i^l$ = molar enthalpy in gas and liquid phases, respectively, for species i, J/(mol i)
$\tilde{H}_{\text{ref}}$ = reference state molar enthalpy, J/mol
$(k_{th})_{\text{air}}, (k_{th})_w$ = thermal conductivity of air and liquid water, respectively, J/(cm s)
k_{yi} = local gas phase mass transfer coefficient for species i, mol i/(cm^2 s)
$\lambda(T_m)$ = partition coefficient for alcohol in water and air
MIGET = multiple inert gas elimination technique
M_w = molecular weight of water, 18.016 g/mol
$\dot{n}$ = convective molar flow rate, mol/s
n_A, n_L = moles of A and liquid, respectively, in mucous control volume, mol
$(\dot{n}_A)_2, (\dot{n}_A)_3$ = diffusion rate of A from tissue to mucus and capillary to tissue, respectively, mol/s
$\dot{n}_i, (\dot{n}_i)_1$ = molar evaporation rate of species i from mucus, mol i/s
$Nu_{\phi,i}$ = Nusselt number, $hD/(k_{\text{th}})_{\text{air}}$
ϕ = phase of respiration
P_A = partial pressure of alcohol, mmHg
Pr = Prandtl number, $\tilde{C}p\mu/k_{\text{th}}$
P_t = total pressure, mmHg
$P(z)$ = airway perimeter at z, cm
$\dot{Q}_{\text{sens}}$ = sensible heat transfer rate from mucosal surface, J/s
$\dot{Q}_2, \dot{Q}_3$ = conductive heat transfer rate from tissue to mucus and capillaries to tissue, respectively, J/s
ρ_w = density of water, g/cm^3
R = universal gas constant, 62360 (ml mmHg)/(mol K)
R = airway radius, cm
ΔR_1 = mucous layer thickness, cm
ΔR_2 = nonperfused tissue thickness, cm
Re = Reynolds number, $\rho\langle v\rangle D/\mu$
RH = relative humidity, %
RHL, RWL = respiratory heat and water loss, respectively, J/min and g/min

$\Delta R_{\min}$ = minimum controlled mucous layer thickness, cm
$\dot{S}_1$ = liquid secretion rate from tissue to mucus, mol/s
$\dot{S}_2$ = liquid filtration rate from capillaries to tissue, mol/s
t = time, s
t_{HC} = half cycle time, s
τ = dimensionless time
T = airway luminal temperature, °C
T_{abs} = absolute temperature of air, K
T_{amb} = ambient air temperature, °C
$(T_{\text{ave}})_1$ = integrated time averaged air temperature, °C
$(T_{\text{ave}})_2$ = arithmetic mean of minimum inspiratory and maximum expiratory air temperature, °C
$T_c(z)$ = capillary bed temperature, °C
T_{head} = temperature of capillary bed in head region, °C
T_m, T_t = temperature of mucus and tissue, respectively, °C
$\tilde{U}_{\text{ref}}$ = reference state molar internal energy, J/mol
U_{tot} = total internal energy in airway control volume, J
$\tilde{U}_i$ = molar internal energy for species i, J/(mol i)
$\dot{V}, \dot{V}_{(z,t)}$ = volumetric flow rate of gas, ml/s
V_T = tidal volume, ml
χ = dimensionless variable
x = dimensional variable
$\langle x_A \rangle$ = average alcohol mole fraction
$(x_A)_c$ = capillary soluble gas mole fraction
x_{Am}, x_{At} = mole fractions of A in mucus and tissue, respectively
$x_{\max}, x_{\min}$ = maximum and minimum values of dimensional variable
y_i = gas phase mole fraction of species i
$y_{i,m}$ = gas phase mole fraction of species i at air/mucus interface
z = axial position from airway entrance, cm